

Online Bayesian State Estimation for Real-Time Monitoring of Growth Kinetics in Thin Film Synthesis

Sumner B. Harris,* Ruth Y. López Fajardo, Alexander A. Puretzky, Kai Xiao, Feng Bao, and Rama K. Vasudevan*



Cite This: *Nano Lett.* 2025, 25, 2444–2451



Read Online

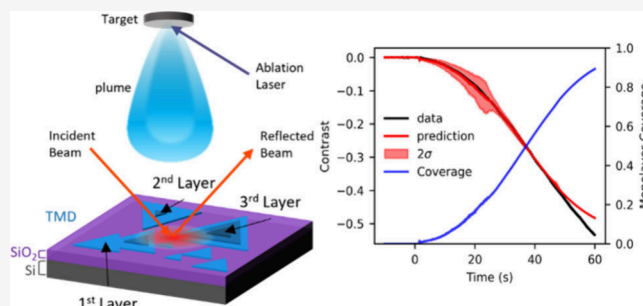
ACCESS |

Metrics & More

Article Recommendations

Supporting Information

ABSTRACT: Rapid validation of newly predicted materials through autonomous synthesis requires real-time adaptive control methods that exploit physics knowledge, a capability that is lacking in most systems. Here, we demonstrate an approach to enable real-time control of thin film synthesis by combining *in situ* optical diagnostics with a Bayesian state estimation method. We developed a physical model for film growth and applied the direct filter (DF) method for real-time estimation of nucleation and growth rates during pulsed laser deposition (PLD). We validated the approach using simulated and experimental reflectivity data for WSe₂ growth and ultimately deployed the algorithm on an autonomous PLD system during the growth of 1T'-MoTe₂. The DF robustly estimates growth parameters in real time at early stages of growth, down to 15% monolayer area coverage. This fusion of *in situ* diagnostics, data assimilation, and physical modeling opens



KEYWORDS: state estimation, thin film synthesis, pulsed laser deposition, real-time control, autonomous synthesis, *in situ* diagnostics

The past decade has seen substantial investment in machine learning and high-throughput computational methodologies for materials science in an endeavor to identify new materials with desirable properties. This is exemplified by the Materials Genome Initiative,¹ which has paved the way for high-throughput computational screening and data-driven research with automated experimentation. Chemical structures can be efficiently navigated *in silico* via high-throughput density functional theory or molecular dynamics. The results of these efforts are stored in vast databases such as the Materials Project,² which machine learning models can utilize to predict candidates for experimental synthesis of new materials.

Despite years of effort, the key obstacle for realizing the potential of such workflows remains the same: predicting new materials is straightforward compared to experimental validation through some synthesis modality. Recent advances in autonomous experiments have increased throughput for synthesis of thin films,^{3–5} nanoparticles,⁶ and bulk powders,⁷ but few efforts have successfully incorporated theory or literature data to narrow the parameter space and inform the commonly used Bayesian optimization loop with physics knowledge. Moreover, many predicted materials are metastable,⁸ which requires that synthesis trajectories be carefully controlled to drive the system toward the desired state. Growth trajectories could be controlled with model-based predictive control⁹ (MPC), which fuses a process model with *in situ*

diagnostics data to predict and adjust a system's trajectory in real time.

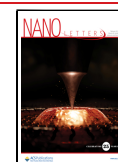
While MPC has been used in chemical synthesis and process control dating back to the 1970s,^{10,11} it is rarely applied in physical vapor deposition (PVD) techniques due to challenges in deriving physical quantities from diagnostic data in real time and the lack of compatible film growth models. For example, reflection high-energy electron diffraction (RHEED) is ubiquitous in molecular beam epitaxy (MBE) and pulsed laser deposition (PLD) to monitor effective growth rates.¹² First MPC-like efforts in PVD date back to 1984 with “phase-locked epitaxy”, where the MBE source shutter is controlled based on oscillations in the RHEED signal.¹³ However, modeling realistic RHEED images from surface structures is an active research area, leading to sporadic efforts to focus on neural network models for prediction and control. Neural networks for MBE control date back to 1993¹⁴ and are typically used with RHEED data to make a predictive model of the future diffraction state¹⁵ as well as pattern classification and

Received: November 21, 2024

Revised: January 14, 2025

Accepted: January 23, 2025

Published: January 29, 2025



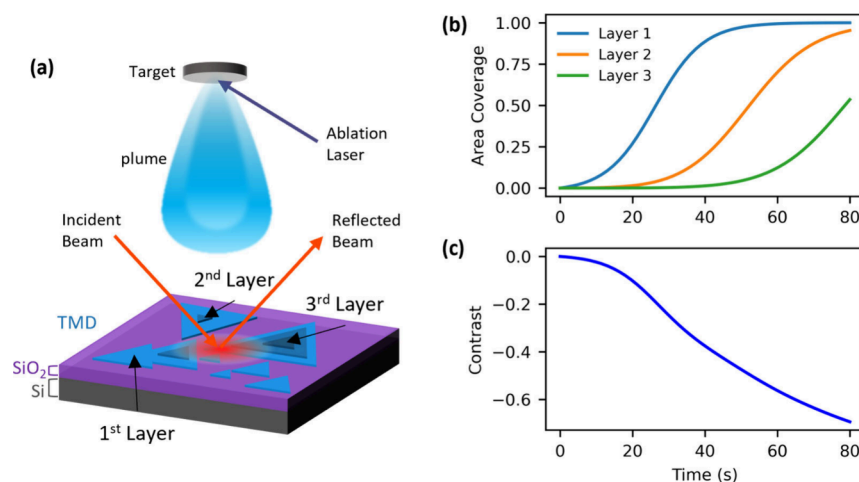


Figure 1. (a) Schematic of pulsed laser deposition of few-layer transition metal dichalcogenides (TMDs) with *in situ* laser reflectivity to monitor growth kinetics. Film growth can be described in terms of fractional area coverage of discrete layers, which nucleate and grow at different rates during deposition. (b) An example of the area coverage vs time for 3 layers of TMD growth based on our autocatalytic growth model. (c) The calculated reflected contrast based on the layer coverage shown in (b) vs time.

clustering, implemented mostly postgrowth.^{16–18} While effective, these approaches still lack interpretability and physics awareness, which are crucial for guiding systems toward the desired states.

To realize physics-informed control over thin film synthesis, different methods are needed to infer the future state of the system. Optical diagnostics are being increasingly adopted in film growth and can be used with simple and accurate physical models, in contrast to RHEED, and provide similar information related to growth rates and composition. *In situ* ellipsometry has been used in an MPC scheme to modulate the composition of Si_{1-x}Ge_x films during chemical vapor deposition (CVD).¹⁹ *In situ* Raman has also been shown to be sensitive to composition and strain during CVD²⁰ and PLD²¹ but has not yet been used for MPC.

Here, we combine *in situ* optical diagnostics with a recently developed Bayesian state estimation method toward enabling MPC of thin film nucleation and growth rates during PLD. We developed a simple and interpretable physical model for thin film growth based on the area coverage of discrete layers, which is measurable by laser reflectivity, and apply the direct filter (DF) method of parameter estimation to determine the growth and nucleation rates of thin films in real time during PLD. We deployed our method on an autonomous PLD system and tested the algorithm in real time during growth of 1T'-MoTe₂. We show that the DF can accurately estimate the growth model parameters at early stages of synthesis and can determine the nucleation and growth rates of the first monolayer after only ~15% area coverage has been deposited. Any physical model describing film growth in the context of an *in situ* diagnostic can be adapted to our method, providing a powerful tool to advance adaptive control in thin film synthesis by integrating modern data assimilation techniques with these diagnostics and physical models.

For the growth of transition metal dichalcogenide (TMD) thin films with PLD, previous work showed that *in situ* laser reflectivity reveals sub-monolayer growth and nucleation kinetics on SiO₂/Si substrates, where the multilayer structure enhances reflected contrast.²² Building on this, we developed a general growth model for an arbitrary number of TMD layers and calculated the reflected contrast using the Fresnel

equations and fractional area coverage of individual layers. We use the same recursive method for calculating the Fresnel reflection coefficient of a homogeneous layer stack and refer to the previous work for a detailed description.²² Thus, our model describes the time evolution of the fractional area coverage for discrete single layers to simulate the experimentally observed reflected contrast.

To describe growth kinetics of 2D materials, we employ a two-step kinetic model that considers conversion of A to B through the nucleation and autocatalytic growth steps described by the rate constants k_n and k_{gr} , respectively.



This approach is the most general and can be applied to interpret sigmoidal kinetics found in many different processes that exhibit cooperative effects when the initial conversion of A to B affects the subsequent conversion process. As shown by Finney et al.,²³ this approach can be used to interpret the parameters of the Avrami equation^{24–26} that was initially developed in the 1940s for kinetics of phase changes as well as its numerous modifications and derivatives (see Finney et al.²³ for review), e.g., for kinetics of diamond film deposition by CVD.²⁷ Here, we apply this growth model to the PLD growth of TMDs.

Figure 1a shows a schematic of the PLD synthesis process and the model used to calculate the contrast. During PLD, a solid target of the desired material is irradiated with a pulsed laser, which creates the vapor phase precursors for film growth. The plume species condense on the SiO₂/Si substrate where monolayer islands begin to nucleate with a rate k_{n1} . Other plume species diffuse along the substrate surface and attach to existing islands at a growth rate of k_{gr1} . The initial area available for a monolayer growth is $f_0(t=0) = 1$ with the initial fractional area coverage of the first monolayer $f_1(t=0) = 0$. As growth continues, additional layers nucleate and grow on top of the first layer islands and so on. This process can be generalized by a system of equations (eq 1), where f_i is the fractional area coverage of layer number i with nucleation and growth rates of k_{ni} and k_{gri} , respectively, up to a total of N

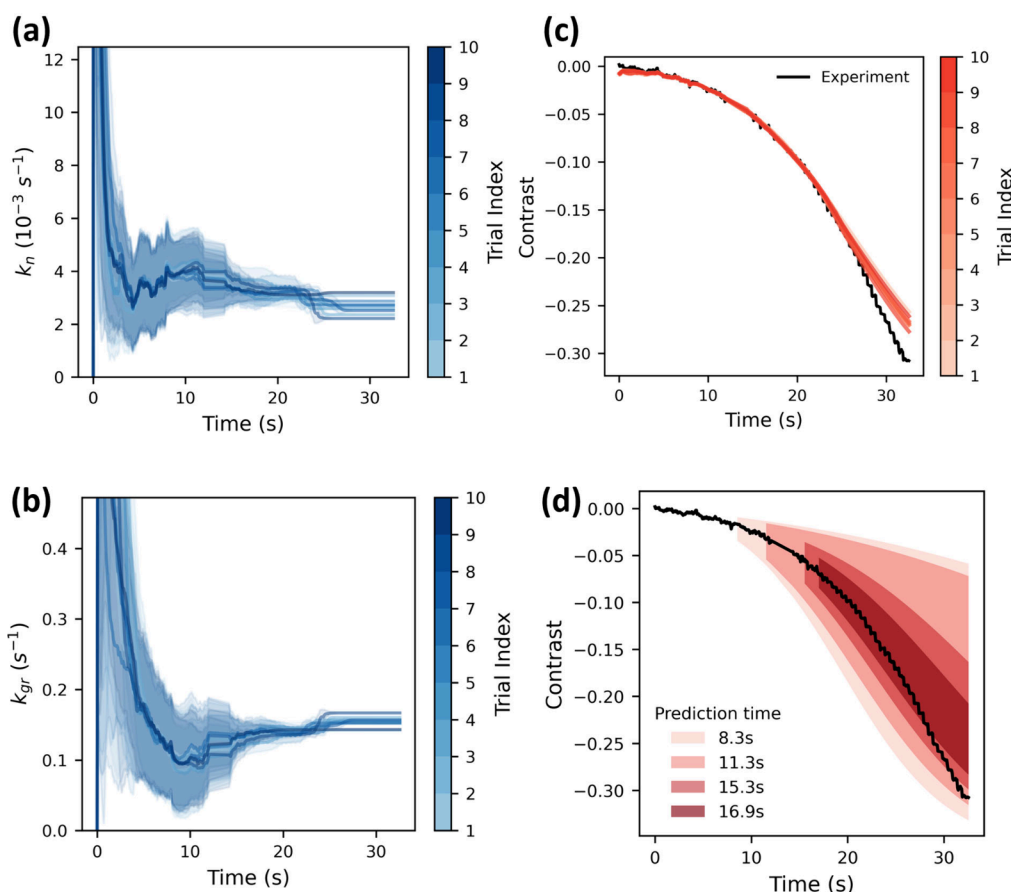


Figure 2. Sequential parameter estimation using experimental data with the monolayer model (eq 3) for 10 trials with an 8 s burn-in period. Each trial is shown as a different color line, where the shaded region represents the uncertainty. (a) Nucleation rate k_n and (b) growth rate k_{gr} are estimated for each sequential time step. (c) The predicted contrast. The average final parameter estimates for this experiment are $k_n = (2.9 \pm 0.3) \times 10^{-3} \text{ s}^{-1}$ and $k_{gr} = 0.147 \pm 0.009 \text{ s}^{-1}$. (d) The projected contrast with uncertainty (shaded area) at four times after the burn-in period.

layers. Here, k_{gr_i} is multiplied by the initial surface area, $A_0 = 1$, to remove the area dependence and to make both rate dimensions s^{-1} . The reflected contrast is given by $C_i = (R_i - R_0)/R_0$ where R_i and R_0 are the Fresnel reflection coefficients of a layer stack with i layers and the bare substrate, respectively. Thus, we can model the time evolution of contrast $C_r(t)$ with eq 2.

$$\frac{df_i}{dt} = k_{ni}(f_{i-1} - f_i) + k_{gr_i}(f_{i-1} - f_i)f_i \text{ where } i = 1, 2, \dots, N \quad (1)$$

$$C_r(t) = \sum_{i=1}^N (C_i - C_{i-1})f_i(t) \quad (2)$$

Figure 1b shows the simulated area coverage vs time for the first 3 TMD layers, while Figure 1c shows the corresponding contrast $C_r(t)$. Equation 1 can be solved numerically for a defined number of layers. For simplified studies of a single monolayer growth, eq 1 is solved analytically (eq 3) where f , k_n , and k_{gr} are the first monolayer coverage and nucleation and growth coefficients, respectively.

$$f(t) = \frac{\frac{k_n}{k_{gr}}(e^{(k_n+k_{gr})t} - 1)}{1 + \frac{k_n}{k_{gr}}e^{(k_n+k_{gr})t}} \quad (3)$$

This model explains the experimental *in situ* reflectivity and allows for online or offline fitting methods to estimate the fundamental nucleation and growth rates for individual layers during PLD. Specifically, we aim to use this model with online, Bayesian methods to estimate the nucleation and growth rates with uncertainty to enable real-time monitoring of these quantities during PLD.

To do this, we consider a state estimation problem where eqs 1 and 2 are the state-space and observation models for film growth, and k_{ni} and k_{gr_i} are the parameters. Here, we are interested in estimating the parameters of the state-space model, rather than the state itself (the contrast), in real time. To do this, we apply the DF method,²⁸ which is a nonlinear particle filtering method that estimates dynamical state-space model parameters.

Filtering methods in data assimilation fuse information from model simulations and observed data within specific time frames. This fusion aims to refine our understanding of a dynamical system and its associated uncertainties recursively in time. Suppose one has the following state-space model $X_{n+1} = G(X_n, \theta) + w_n$, $n = 1, 2, 3, \dots$, where $G(X_n, \theta)$ is the dynamical model describing the evolution of the state process X_n at time step n defined by the state parameters θ , where w_n represents additive noise. In addition, we have an observation model $Y_{n+1} = H(X_{n+1}) + \xi_{n+1}$, where H represents the observation function and ξ_{n+1} is observation noise. The DF method considers the model parameters θ as the only state to estimate. Since the

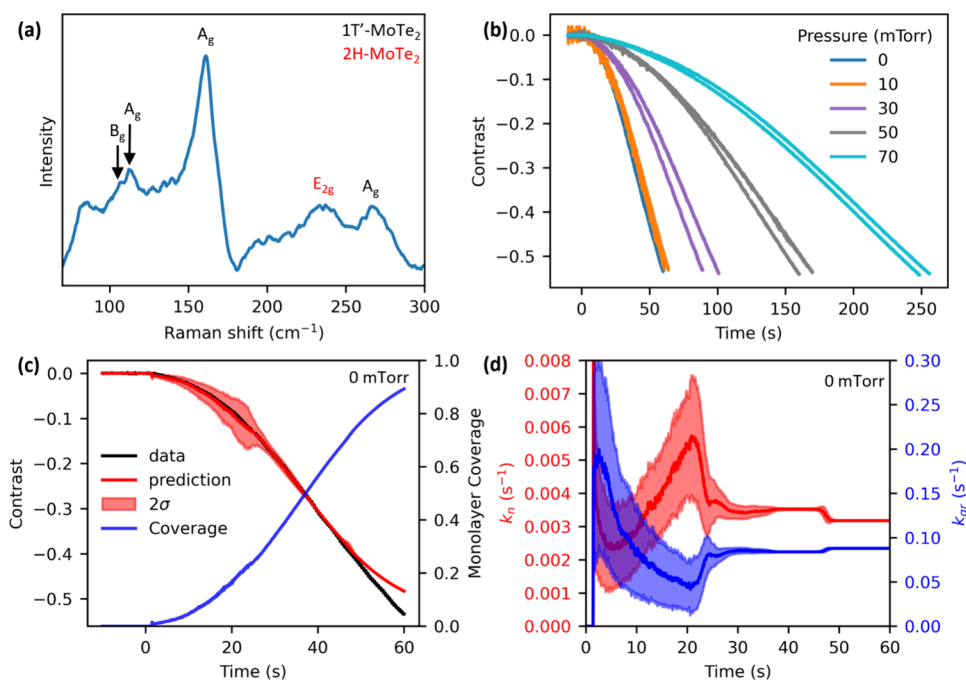


Figure 3. Application of real-time direct filter (DF) parameter estimation during PLD synthesis of ~ 1 monolayer thick $1T'$ - MoTe_2 films grown at 200°C with various Ar background pressures between vacuum ($<1 \times 10^{-6}$ Torr) and 70 mTorr. (a) Raman spectrum of a ~ 10 layer thick film indicating the predominant phase is the metallic $1T'$ with some semiconducting $2H$ present. (b) Laser reflectivity contrast curves showing the difference in growth rates at different pressures, with some run-to-run variability. (c) Detailed view of contrast curve for the film grown at vacuum comparing the experimental data (black) with the DF predictions (red) and the monolayer area coverage (blue). The envelope around the DF predictions is the uncertainty (\pm std. dev., σ). (d) DF-predicted growth and nucleation rates, k_n and k_{gr} , with uncertainty vs time.

observation process does not directly measure the parameters, the DF composites the state model into the observation function to construct the nonlinear filtering problem given by eqs 4a and 4b where ϵ_n is the additive Gaussian noise.

$$\theta_{n+1} = \theta_n + \epsilon_n \quad (4a)$$

$$Y_{n+1} = H(G(X_n, \theta_{n+1}) + w_n) + \xi_{n+1} \quad (4b)$$

Details of the DF implementation used in this work are given in the Supporting Information (Note S1). We first apply DF estimation to simulated data generated using the monolayer model (eq 3) to estimate the known k_n and k_{gr} of WSe_2 monolayers to evaluate the efficacy of this approach. We find that the DF can accurately estimate the rate parameters when using a “burn-in” period that sets the artificial noise to $\epsilon_n = 0$ after a short time. Full details of this simulated data study are given in the Supporting Information (Note S2, Figure S1).

We test the DF method with previously acquired experimental data that was collected during an autonomous WSe_2 growth experiment.⁵ Figure 2a–c show the sequential estimation of k_n and k_{gr} along with the predicted contrast for experimental data. We repeated the estimation 10 times with a different random seed to check repeatability using a burn-in time of 8 s. We observe similar convergent behavior to those in the simulated data case (Figure S1) and find the 10-trial average values of $k_n = (2.9 \pm 0.3) \times 10^{-3} \text{ s}^{-1}$ and $k_{gr} = 0.147 \pm 0.009 \text{ s}^{-1}$. This method enables projection of the contrast curve to future times, which is one possible application during online estimation. We take the parameter estimates at fixed times after the burn-in period and project the contrast forward with the uncertainty. Figure 2d shows the results of these projections at 8.3, 11.3, 15.3, and 16.9 s. The uncertainty is high immediately after burn-in but decreases as more data are collected. The

projections at 15.3 and 16.9 s (approximately twice the burn-in time) both have a small enough uncertainty that they could be used to reasonably predict the final growth time and rates with enough remaining time to make changes to the experimental parameters and alter the course of growth. The contrast at these two times corresponds to 15% and 19% monolayer area coverage and correspond to a difference of only 2 or 3 laser pulses. At these low coverages and at the lower limit of deposition control via the laser pulse number, we anticipate that intervening in the experiment at this time by changing the repetition rate, laser fluence, or substrate temperature could meaningfully alter the future growth and resulting properties of the film.

Notably, the predicted contrast deviates from the experimental measurements at later times (Figure 2c). This is due to the nucleation of additional layers beyond the first monolayer, whose fractional area coverage begins to significantly contribute to the reflected contrast. We previously found that beyond $\sim 40\%$ monolayer coverage, the second layer begins to nucleate.²² Indeed, the contrast at which the experiment deviates from the monolayer growth model, at ~ 25 s, corresponds to 45% monolayer coverage, so we can anticipate second layer nucleation.

To our knowledge, state estimation methods, such as the one developed in this work, have never been deployed on any PLD system. Other Bayesian techniques have been used primarily for sequential design of experiments (Bayesian optimization) in synthesis^{3–5} to achieve some target metric in a small number of experiments. In this case, the DF method is not used for active learning or experimental design but rather uses the calculated probability distributions of the growth model parameters to accurately estimate their values with a small amount of data. To demonstrate this application in a real

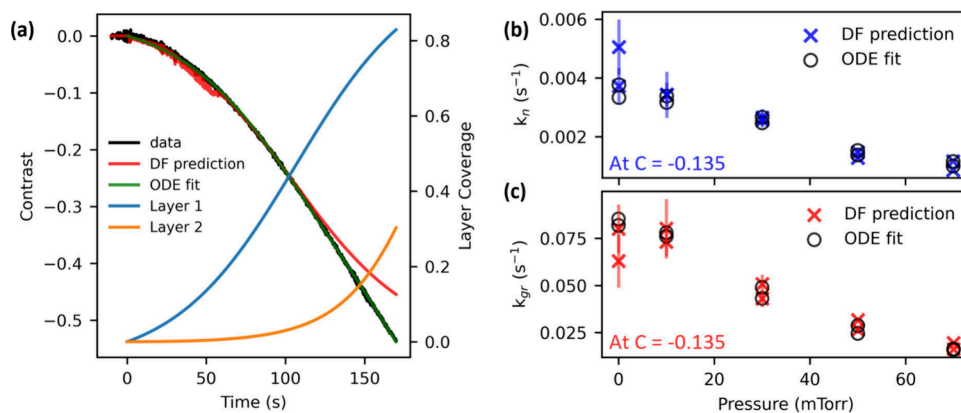


Figure 4. Comparison of real-time direct filter (DF) parameter estimation with post-growth fitting with a 2-layer model. (a) Contrast curve during PLD growth of MoTe₂ at 50 mTorr overlaid with the real-time DF predictions and the post-growth 2-layer model fit (ODE fit) (left axis). The individual layer coverages from the ODE fit (right axis) show that the monolayer DF model begins to diverge from the data as layer 2 begins to grow, as expected. The nucleation rate k_n (b) and growth rate k_{gr} (c) for layer 1 vs Ar pressure determined from the DF and ODE fits closely match. The ODE fit requires all the data (post-growth analysis), while the rates shown in (b) and (c) for the DF were taken from the point of each curve when the contrast reached -0.135 ($\sim 25\%$ monolayer coverage). The DF parameter estimation can capture the growth kinetic parameters accurately in real time at early stages of film growth.

PLD environment, we integrated the above monolayer growth model and DF algorithm into the control software for an autonomous PLD system⁵ and grew ultrathin films of 1T'-MoTe₂ at different Ar background pressures to test the reliability of real-time parameter estimation under conditions with different deposition rates. We synthesized 2 films at 5 different pressures between vacuum ($<1 \times 10^{-6}$ Torr) and 70 mTorr with all other deposition variables and DF algorithm parameters held constant; details are given in the [Supporting Information](#). Deposition was automatically terminated when the contrast reached the value expected for a monolayer of 1T'-MoTe₂, which was -0.54 .

MoTe₂ can crystallize in three different phases: the hexagonal semiconducting 2H phase, the monoclinic metallic 1T' phase, or the orthorhombic T_d phase, which exhibits quantum type-II Weyl semimetal behavior²⁹ and superconductivity.³⁰ The 2H phase is the most thermodynamically stable, but the energy difference between the 2H and 1T' phases is the lowest of all TMDs at only ~ 35 meV.³¹ The 1T' phase forms at higher growth temperatures³² and under Te-deficient conditions,³³ while the T_d phase becomes the most stable at high temperatures³⁴ compared to the 2H phase. Therefore, MoTe₂ is an ideal material system for exploring synthesis methodologies to tune the phase compositions of thin films. Although no direct growth of MoTe₂ by PLD has been reported, there are two studies on PLD-deposited amorphous (Mo,W)Te_{2-x} alloys at room temperature with post-growth annealing.^{35,36}

Figure 3a shows the Raman spectrum of a typical thick film (~ 10 layers) of MoTe₂ grown at 200 °C. The spectrum indicates that the films crystallize predominantly in the 1T' phase, with the main A_g modes of 1T'-MoTe₂ at 161 and 266 cm^{-1} and broad peaks in the vicinity of the B_g mode at 107 cm^{-1} and A_g mode at 110 cm^{-1} , consistent with literature.^{37,38} The weaker Raman peaks are not resolvable; therefore, we refer to only the general regions expected for these modes. This spectrum is similar to nanostructured 1T' films³⁹ and also the Te-deficient films in Sun et al.³⁵ Interestingly, the 2H phase should be more stable than the 1T' phase below ~ 300 °C.⁴⁰ The 1T' phase is the dominant phase in our case due to Te deficiency, most likely caused by incommensurate evaporation

of Mo and Te during ablation. It has been shown that excess Te is required to stabilize the 2H phase and that the 1T' phase forms otherwise.^{33,41} Film optimization and properties are not the topics of this work and will be left to future studies. Here, knowledge of the primary crystal phase is required to select the correct optical constants to conduct the DF experiments. We selected the refractive index of 1T'-MoTe₂ in this case, given in the [Supporting Information](#).

Figure 3b shows the real-time reflected contrast during each growth. The number of pulses needed to grow ~ 1 monolayer ranges from 120 in a vacuum to 512 at 70 mTorr, with run-to-run variation likely caused by changes in the target surface that modulate the ablation yield with each laser pulse. DF parameter estimation was performed in real time without tuning the DF algorithm parameters during the synthesis of all 10 samples, demonstrating its robustness across various growth rates. **Figure 3c** details one sample grown in vacuum, where DF contrast predictions (red) with a 2σ uncertainty envelope (± 1 standard deviation σ) are compared to monolayer area coverage (blue). DF predictions deviate from the experimental data at ~ 49.5 s, aligning with $\sim 76\%$ monolayer coverage, beyond which we expect significant contributions from additional layers that the model does not consider. **Figure 3d** shows that parameter predictions stabilize after ~ 19.5 s, with final predicted rates of $k_n = 3.18 \times 10^{-3} \text{ s}^{-1}$ and $k_{gr} = 8.78 \times 10^{-2} \text{ s}^{-1}$. The smaller k_{gr}/k_n ratio of 27.6 for 1T'-MoTe₂ compared to WSe₂ (50.7) can explain the higher monolayer coverage (76% vs 40%) before additional layer nucleation.

Finally, we compared real-time DF rate predictions with post-growth analysis to determine if the rates are accurately predicted prior to the end of film growth. Using a two-layer model (eqs 1 and 2), we fit all 10 MoTe₂ contrast curves, solving the equations via integration (SciPy⁴² odeint) and minimizing MSE as a function of k_{ni} and k_{gr} (ODE fit). **Figure 4a** shows one 50 mTorr 1T'-MoTe₂ deposition, with real-time DF predictions overlaid with the ODE fit results. Both methods fit the data well, though the DF deviates when the second layer forms, as previously noted. The key difference is that the DF is done in real time as data is received from the detector, whereas the ODE fit requires the whole curve. **Figure 4b,c** display k_n and k_{gr} vs Ar pressure for layer 1 using DF

estimation at $\sim 25\%$ monolayer coverage (contrast of -0.135) for each deposition compared with the results from the ODE fit results. DF accurately matches the postgrowth ODE fits, even with partial data early in the deposition. Thus, this method is highly effective for tracking growth kinetics in real time, supporting future autonomous optimization during thin film synthesis via PLD.

We applied an online Bayesian state estimation technique called the direct filter method to estimate the parameters of a thin film growth kinetics model in real time during PLD of ultrathin TMD materials. The DF estimates the growth and nucleation rate parameters of a growth model based on the area coverage of discrete layers, measurable with *in situ* laser reflectivity. We tested the method on simulated and previously acquired data for WSe_2 growth and ultimately deployed the algorithm on an autonomous PLD system to demonstrate real-time parameter estimation during the automated growth of $1\text{T}'\text{-MoTe}_2$. The DF method robustly estimates model parameters at early stages of growth with accuracy consistent with postgrowth analysis. By combining *in situ* diagnostics with a physical model, real-time control in PLD becomes feasible. Moving forward, achieving real-time control of the physical growth parameters during synthesis can be done through several approaches, depending on the experimental goals, desired level of physical insight, and available experimental automation. Simple reactive methods like proportional-integral-derivative (PID) control can be used with a single synthesis parameter to maintain a nucleation or growth rate set point. A more advanced and physically insightful method would be to express the rates as explicit functions of the synthesis parameters and define operating bounds for each to achieve a desired nucleation or growth rate. The functional forms of the rates would need to be derived theoretically, or a neural surrogate function could be constructed through active learning experiments. Finally, reinforcement learning could be used to autonomously learn an optimized control strategy over the course of numerous synthesis experiments. Extending this approach to more complex growth models and additional *in situ* techniques (RHEED, ellipsometry, etc.) enables control of different film qualities, such as crystal phase or refractive index. Combining these control strategies with online parameter estimation methods like the DF holds promise for achieving true control of synthesis for thin films and may finally enable tailored synthesis of desired metastable phases that are very difficult or impossible to reliably fabricate using existing methodologies.

■ ASSOCIATED CONTENT

Data Availability Statement

The data that support the findings of this study are openly available at <https://github.com/sumner-harris/PLD-Direct-Filter.git>

SI Supporting Information

The Supporting Information is available free of charge at <https://pubs.acs.org/doi/10.1021/acs.nanolett.4c05921>.

Details of the direct filter method for parameter estimation; results of parameter estimation for simulated data; experimental methods (PDF)

Accession Codes

The data that support the findings of this study are openly available at <https://github.com/sumner-harris/PLD-Direct-Filter.git>

■ AUTHOR INFORMATION

Corresponding Authors

Sumner B. Harris – Center for Nanophase Materials Sciences, Oak Ridge National Laboratory, Oak Ridge, Tennessee 37831, United States; orcid.org/0000-0003-4905-0482; Email: harrisb@ornl.gov

Rama K. Vasudevan – Center for Nanophase Materials Sciences, Oak Ridge National Laboratory, Oak Ridge, Tennessee 37831, United States; orcid.org/0000-0003-4692-8579; Email: vasudevanrk@ornl.gov

Authors

Ruth Y. López Fajardo – Department of Mathematics, Florida State University, Tallahassee, Florida 32306, United States

Alexander A. Puzetky – Center for Nanophase Materials Sciences, Oak Ridge National Laboratory, Oak Ridge, Tennessee 37831, United States; orcid.org/0000-0002-9996-4429

Kai Xiao – Center for Nanophase Materials Sciences, Oak Ridge National Laboratory, Oak Ridge, Tennessee 37831, United States; orcid.org/0000-0002-0402-8276

Feng Bao – Department of Mathematics, Florida State University, Tallahassee, Florida 32306, United States

Complete contact information is available at: <https://pubs.acs.org/10.1021/acs.nanolett.4c05921>

Author Contributions

S.B.H.: Conceptualization (lead); investigation (equal); data curation (lead); methodology (equal); software (lead); visualization (lead) writing—original draft (lead); writing—review and editing (lead). R.F.: Methodology (equal); investigation (equal); software (supporting); writing—original draft (supporting); writing—review and editing (supporting). A.A.P.: Methodology (equal); investigation (equal); writing—original draft (supporting). K.X.: writing—review and editing (supporting) F.B.: Methodology (equal); writing—review and editing (supporting). R.K.V.: writing—original draft (supporting); conceptualization (supporting); writing—review and editing (supporting). All authors read and approved the final manuscript.

Notes

The authors declare no competing financial interest. This manuscript has been authored by UT-Battelle, LLC, under Contract No. DE-AC05-00OR22725 with the U.S. Department of Energy. The United States Government retains and the publisher, by accepting the article for publication, acknowledges that the United States Government retains a nonexclusive, paid-up, irrevocable, worldwide license to publish or reproduce the published form of this manuscript, or allow others to do so, for United States Government purposes. The Department of Energy will provide public access to these results of federally sponsored research in accordance with the DOE Public Access Plan (<http://energy.gov/downloads/doe-public-access-plan>).

■ ACKNOWLEDGMENTS

The algorithm development and machine learning were supported by the Center for Nanophase Materials Sciences (CNMS), which is a U.S. Department of Energy, Office of Science User Facility, at Oak Ridge National Laboratory, and materials synthesis and modeling was supported by the U.S.

Department of Energy, Office of Science, Basic Energy Sciences, Materials Sciences and Engineering Division. F. Bao would like to acknowledge the support from U.S. National Science Foundation through project DMS-2142672 and the support from the U.S. Department of Energy, Office of Science, Office of Advanced Scientific Computing Research, Applied Mathematics program, under Grant DE-SC0025412.

REFERENCES

- (1) *Materials Genome Initiative for Global Competitiveness*; Executive Office of the President, National Science and Technology Council, 2011.
- (2) Jain, A.; Ong, S. P.; Hautier, G.; Chen, W.; Richards, W. D.; Dacek, S.; Cholia, S.; Gunter, D.; Skinner, D.; Ceder, G.; Persson, K. A. Commentary: The Materials Project: A Materials Genome Approach to Accelerating Materials Innovation. *APL Materials* **2013**, *1*, 10110022013.
- (3) MacLeod, B. P.; Parlane, F. G. L.; Morrissey, T. D.; Häse, F.; Roch, L. M.; Dettelbach, K. E.; Moreira, R.; Yunker, L. P. E.; Rooney, M. B.; Deeth, J. R.; Lai, V.; Ng, G. J.; Situ, H.; Zhang, R. H.; Elliott, M. S.; Haley, T. H.; Dvorak, D. J.; Aspuru-Guzik, A.; Hein, J. E.; Berlinguette, C. P. Self-Driving Laboratory for Accelerated Discovery of Thin-Film Materials. *Science Advances* **2020**, *6*, No. eaaz8867.
- (4) Shimizu, R.; Kobayashi, S.; Watanabe, Y.; Ando, Y.; Hitosugi, T. Autonomous Materials Synthesis by Machine Learning and Robotics. *APL Materials* **2020**, *8*, 111110.
- (5) Harris, S. B.; Biswas, A.; Yun, S. J.; Roccapiore, K. M.; Rouleau, C. M.; Puzos, A. A.; Vasudevan, R. K.; Geohegan, D. B.; Xiao, K. Autonomous Synthesis of Thin Film Materials with Pulsed Laser Deposition Enabled by in Situ Spectroscopy and Automation. *Small Methods* **2024**, *8*, 2301763.
- (6) Volk, A. A.; Epps, R. W.; Yonemoto, D. T.; Masters, B. S.; Castellano, F. N.; Reyes, K. G.; Abolhasani, M. Alphaflow: Autonomous Discovery and Optimization of Multi-Step Chemistry Using a Self-Driven Fluidic Lab Guided by Reinforcement Learning. *Nat. Commun.* **2023**, *14*, 1403.
- (7) Szymanski, N. J.; Rendy, B.; Fei, Y.; Kumar, R. E.; He, T.; Milsted, D.; McDermott, M. J.; Gallant, M.; Cubuk, E. D.; Merchant, A.; Kim, H.; Jain, A.; Bartel, C. J.; Persson, K.; Zeng, Y.; Ceder, G. An Autonomous Laboratory for the Accelerated Synthesis of Novel Materials. *Nature* **2023**, *624*, 86–91.
- (8) Therrien, F.; Jones, E. B.; Stevanović, V. Metastable Materials Discovery in the Age of Large-Scale Computation. *Applied Physics Reviews* **2021**, *8*, 031310(2021) DOI: 10.1063/5.0049453.
- (9) Schwenzer, M.; Ay, M.; Bergs, T.; Abel, D. Review on Model Predictive Control: An Engineering Perspective. *International Journal of Advanced Manufacturing Technology* **2021**, *117*, 1327–1349.
- (10) Richalet, J.; Rault, A.; Testud, J. L.; Papon, J. Model Predictive Heuristic Control: Applications to Industrial Processes. *Automatica* **1978**, *14*, 413–428.
- (11) Cutler, C. R.; Ramaker, B. L. Dynamic matrix control. A computer control algorithm. *Joint Automatic Control Conference* **1980**, *17*, 72.
- (12) Ichimiya, A.; Cohen, P. I. *Reflection High-Energy Electron Diffraction* (Cambridge University Press, 2004).
- (13) Sakamoto, T.; Funabashi, H.; Ohta, K.; Nakagawa, T.; Kawai, N. J.; Kojima, T. Phase-Locked Epitaxy Using Rheed Intensity Oscillation. *Jpn. J. Appl. Phys.* **1984**, *23*, L657.
- (14) Currie, K. R.; LeClair, S. R. Self-Improving Process Control for Molecular Beam Epitaxy. *International Journal of Advanced Manufacturing Technology* **1993**, *8*, 244–251.
- (15) Lee, K. K.; Brown, T.; Dagnall, G.; Bicknell-Tassius, R.; Brown, A.; May, G. S. Using Neural Networks to Construct Models of the Molecular Beam Epitaxy Process. *IEEE Transactions on Semiconductor Manufacturing* **2000**, *13*, 34–45.
- (16) Shen, C.; Zhan, W.; Xin, K.; Li, M.; Sun, Z.; Cong, H.; Xu, C.; Tang, J.; Wu, Z.; Xu, B.; Wei, Z.; Xue, C.; Zhao, C.; Wang, Z. Machine-Learning-Assisted and Real-Time-Feedback-Controlled Growth of InAs/GaSb Quantum Dots. *Nat. Commun.* **2024**, *15*, 2724.
- (17) Liang, H.; Stanev, V.; Kusne, A. G.; Tsukahara, Y.; Ito, K.; Takahashi, R.; Lippmaa, M.; Takeuchi, I. Application of Machine Learning to Reflection High-Energy Electron Diffraction Images for Automated Structural Phase Mapping. *Physical Review Materials* **2022**, *6*, 063805.
- (18) Provence, S. R.; Thapa, S.; Paudel, R.; Truttman, T. K.; Prakash, A.; Jalan, B.; Comes, R. B. Machine Learning Analysis of Perovskite Oxides Grown by Molecular Beam Epitaxy. *Physical Review Materials* **2020**, *4*, 083807.
- (19) Middlebrooks, S. A.; Rawlings, J. B. Model Predictive Control of Si_{1-x}Ge_x Thin Film Chemical-Vapor Deposition. *IEEE Transactions on Semiconductor Manufacturing* **2007**, *20*, 114–125.
- (20) Qin, Y.; Sayyad, M.; Montblanch, A. R.-P.; Feuer, M. S. G.; Dey, D.; Blei, M.; Sailus, R.; Kara, D. M.; Shen, Y.; Yang, S.; Botana, A. S.; Atature, M.; Tongay, S. Reaching the Excitonic Limit in 2d Janus Monolayers by in Situ Deterministic Growth. *Adv. Mater.* **2022**, *34*, 2106222.
- (21) Harris, S. B.; Lin, Y.-C.; Puzos, A. A.; Liang, L.; Dyck, O.; Berlijn, T.; Eres, G.; Rouleau, C. M.; Xiao, K.; Geohegan, D. B. Real-Time Diagnostics of 2d Crystal Transformations by Pulsed Laser Deposition: Controlled Synthesis of Janus WsSe Monolayers and Alloys. *ACS Nano* **2023**, *17*, 2472–2486.
- (22) Puzos, A. A.; Lin, Y.-C.; Liu, C.; Strasser, A. M.; Yu, Y.; Canulescu, S.; Rouleau, C. M.; Xiao, K.; Duscher, G.; Geohegan, D. B. In Situ Laser Reflectivity to Monitor and Control the Nucleation and Growth of Atomically Thin 2d Materials*. *2D Materials* **2020**, *7*, 025048.
- (23) Finney, E. E.; Finke, R. G. Is There a Minimal Chemical Mechanism Underlying Classical Avrami-Erofe'ev Treatments of Phase-Transformation Kinetic Data? *Chem. Mater.* **2009**, *21*, 4692–4705.
- (24) Avrami, M. Kinetics of Phase Change. I General Theory. *J. Chem. Phys.* **1939**, *7*, 1103–1112.
- (25) Avrami, M. Kinetics of Phase Change. II Transformation-Time Relations for Random Distribution of Nuclei. *J. Chem. Phys.* **1940**, *8*, 212–224.
- (26) Avrami, M. Granulation, Phase Change, and Microstructure Kinetics of Phase Change. III. *J. Chem. Phys.* **1941**, *9*, 177–184.
- (27) Tomellini, M. Coverage-Time Dependence during Island Growth at a Solid Surface with Application to Diamond Deposition from the Gas Phase. *J. Appl. Phys.* **1992**, *72*, 1589–1594.
- (28) Archibald, R.; Bao, F.; Tu, X. A Direct Filter Method for Parameter Estimation. *J. Comput. Phys.* **2019**, *398*, 108871.
- (29) Jiang, J.; Liu, Z. K.; Sun, Y.; Yang, H. F.; Rajamathi, C. R.; Qi, Y. P.; Yang, L. X.; Chen, C.; Peng, H.; Hwang, C. C.; Sun, S. Z.; Mo, S. K.; Vobornik, I.; Fujii, J.; Parkin, S. S. P.; Felser, C.; Yan, B. H.; Chen, Y. L. Signature of Type-II Weyl Semimetal Phase in Mote₂. *Nat. Commun.* **2017**, *8*, 13973.
- (30) Qi, Y.; Naumov, P. G.; Ali, M. N.; Rajamathi, C. R.; Schnelle, W.; Barkalov, O.; Hanfland, M.; Wu, S.-C.; Shekhar, C.; Sun, Y.; Süß, V.; Schmidt, M.; Schwarz, U.; Pippel, E.; Werner, P.; Hillebrand, R.; Förster, T.; Kampert, E.; Parkin, S.; Cava, R. J.; et al. Superconductivity in Weyl Semimetal Candidate Mote₂. *Nat. Commun.* **2016**, *7*, 11038.
- (31) He, H.-K.; Jiang, Y.-B.; Yu, J.; Yang, Z.-Y.; Li, C.-F.; Wang, T.-Z.; Dong, D.-Q.; Zhuge, F.-W.; Xu, M.; Hu, Z.-Y.; Yang, R.; Miao, X.-S. Ultrafast and Stable Phase Transition Realized in Mote₂-Based Memristive Devices. *Materials Horizons* **2022**, *9*, 1036–1044.
- (32) Sung, J. H.; Heo, H.; Si, S.; Kim, Y. H.; Noh, H. R.; Song, K.; Kim, J.; Lee, C.-S.; Seo, S.-Y.; Kim, D.-H.; Kim, H. K.; Yeom, H. W.; Kim, T.-H.; Choi, S.-Y.; Kim, J. S.; Jo, M.-H. Coplanar Semiconductor–Metal Circuitry Defined on Few-Layer Mote₂ Via Polymorphic Heteroepitaxy. *Nat. Nanotechnol.* **2017**, *12*, 1064–1070.
- (33) Park, J. C.; Yun, S. J.; Kim, H.; Park, J.-H.; Chae, S. H.; An, S.-J.; Kim, J.-G.; Kim, S. M.; Kim, K. K.; Lee, Y. H. Phase-Engineered Synthesis of Centimeter-Scale 1t' and 2h-Molybdenum Ditetelluride Thin Films. *ACS Nano* **2015**, *9*, 6548–6554.

(34) Ryu, H.; Lee, Y.; Kim, H.-J.; Kang, S.-H.; Kang, Y.; Kim, K.; Kim, J.; Janicek, B. E.; Watanabe, K.; Taniguchi, T.; Huang, P. Y.; Cheong, H.; Jung, I.-H.; Kim, K.; Son, Y.-W.; Lee, G.-H. Anomalous Dimensionality-Driven Phase Transition of MoTe_2 in Van Der Waals Heterostructure. *Adv. Funct. Mater.* **2021**, *31*, 2107376.

(35) Sun, W.; Chen, Y.; Zhuang, W.; Chen, Z.; Song, A.; Liu, R.; Wang, X. Sizable Spin-to-Charge Conversion in PLD-Grown Amorphous $(\text{Mo}, \text{W})\text{Te}_{2-x}$ Films. *Nanotechnology* **2023**, *34*, 135001.

(36) Chen, Y.; Chen, Y.; Ning, J.; Chen, L.; Zhuang, W.; He, L.; Zhang, R.; Xu, Y.; Wang, X. Observation of Shubnikov-De Haas Oscillations in Large-Scale Weyl Semimetal WTe_2 Films. *Chin. Phys. Lett.* **2020**, *37*, 017104.

(37) Ma, X.; Guo, P.; Yi, C.; Yu, Q.; Zhang, A.; Ji, J.; Tian, Y.; Jin, F.; Wang, Y.; Liu, K.; Xia, T.; Shi, Y.; Zhang, Q. Raman Scattering in the Transition-Metal Dichalcogenides of $1\text{T}'\text{-MoTe}_2$, $\text{T}_d\text{-MoTe}_2$, and $\text{T}_d\text{-WTe}_2$. *Phys. Rev. B* **2016**, *94*, 214105.

(38) Beams, R.; Cançado, L. G.; Krylyuk, S.; Kalish, I.; Kalanyan, B.; Singh, A. K.; Choudhary, K.; Bruma, A.; Vora, P. M.; Tavazza, F.; Davydov, A. V.; Stranick, S. J. Characterization of Few-Layer $1\text{T}'\text{-MoTe}_2$ by Polarization-Resolved Second Harmonic Generation and Raman Scattering. *ACS Nano* **2016**, *10*, 9626–9636.

(39) Sun, Y.; Wang, Y.; Sun, D.; Carvalho, B. R.; Read, C. G.; Lee, C.-h.; Lin, Z.; Fujisawa, K.; Robinson, J. A.; Crespi, V. H.; Terrones, M.; Schaak, R. E. Low-Temperature Solution Synthesis of Few-Layer $1\text{T}'\text{-MoTe}_2$ Nanostructures Exhibiting Lattice Compression. *Angew. Chem. Int. Ed.* **2016**, *55*, 2830–2834.

(40) Empante, T. A.; Zhou, Y.; Klee, V.; Nguyen, A. E.; Lu, I. H.; Valentin, M. D.; Naghibi Alvillar, S. A.; Preciado, E.; Berges, A. J.; Merida, C. S.; Gomez, M.; Bobek, S.; Isarraraz, M.; Reed, E. J.; Bartels, L. Chemical Vapor Deposition Growth of Few-Layer MoTe_2 in the 2h , $1\text{t}'$, and 1t Phases: Tunable Properties of MoTe_2 Films. *ACS Nano* **2017**, *11*, 900–905.

(41) Keum, D. H.; Cho, S.; Kim, J. H.; Choe, D.-H.; Sung, H.-J.; Kan, M.; Kang, H.; Hwang, J.-Y.; Kim, S. W.; Yang, H.; Chang, K. J.; Lee, Y. H. Bandgap Opening in Few-Layered Monoclinic MoTe_2 . *Nat. Phys.* **2015**, *11*, 482–486.

(42) Virtanen, P.; Gommers, R.; Oliphant, T. E.; Haberland, M.; Reddy, T.; Cournapeau, D.; Burovski, E.; Peterson, P.; Weckesser, W.; Bright, J.; et al. Scipy 1.0: Fundamental Algorithms for Scientific Computing in Python. *Nat. Methods* **2020**, *17*, 261–272.